Journal of Materials Science: Materials in Medicine (2020)31:12
https://doi.org/10.1007/s10856-019-6352-5

BIOMATERIALS SYNTHESIS AND CHARACTERIZATION

Original Research

Synthesis and characterization of novel calcium phosphate glass-derived cements for vital pulp therapy

Jerry Howard[1] · Levi Gardner[1] · Zahra Saifee[1] · Aladdin Geleil[2] · Isaac Nelson[3] · John S. Colombo[4] · Steven E. Naleway[3] · Krista Carlson[1]

Received: 28 August 2019 / Accepted: 19 December 2019

Abstract

Evaluation of the physicochemical behavior and setting reactions of a novel inorganic pulp capping cement which makes use of the unique corrosion properties of sodium metasilicate (NaSi) glass. NaSi and calcium phosphate (CaP) glass powders were synthesized through a melt-quench method. Cements were created by mixing various amounts of the glasses with deionized water at a powder-to-liquid ratio of 2.5 g mL^{-1}. Working and setting times were measured using the indentation standard ISO 9917-1. Sealing ability was tested by placing set samples of each composition in methylene blue dye solution for 24 h. Set samples were also submerged in phosphate buffered saline and incubated at 37 °C for one week. X-ray diffraction was used to identify mature crystalline phases after incubation. Infrared spectroscopy and scanning electron microscopy were used to characterize cements before and after setting and after incubation. Working and setting times measured in the ranges of 2–5 and 10–25 min, respectively. Working and setting time generally decrease with increased NaSi concentration. Cements with compositions of 25 and 33 wt% NaSi were found to resist the infiltration of dye and maintain their shape. Compositions outside this range absorbed dye and collapsed. Infrared spectroscopy provided insight into the setting mechanism of these cements. After one week in vitro, cements were found to contain crystalline phases matching chemically stable, bioactive phases. The combination of NaSi and CaP glasses has favorable setting behavior, sealing ability, and mature phases for pulp capping while relying on a relatively simple, inorganic composition.

Graphical Abstract

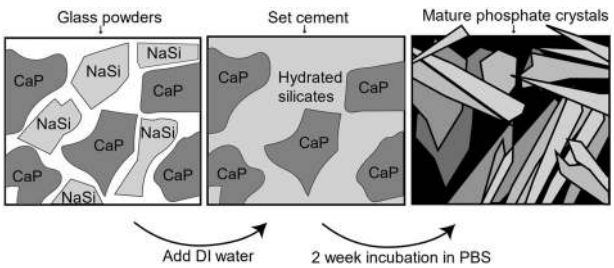

✉ Jerry Howard
jrhow2@gmail.com

✉ Krista Carlson
krista.carlson@utah.edu

[1] University of Utah Materials Science and Engineering, 135S 1460 E RM 202, Salt Lake City, UT 84112, USA

[2] White Engineering Surfaces Corporation, 1 Pheasant Run, Newtown, PA 18940, USA

[3] University of Utah Mechanical Engineering, 1495 E 100S RM2157, Salt Lake City, UT 84112, USA

[4] Nevada School of Dentistry, University of Las Vegas, 1001 Shadow Ln, Las Vegas, NV 89106, USA

Published online: 02 January 2020

1 Introduction

Tooth decay, also known as dental caries or cavities, is the most common chronic disease among children and prevalent in all age groups as well [1]. In the Unites States, the disease affects 92% of the population between ages 16 and 65, and the failure rate of dental restorations within 10 years is approximately 50% [2]. Failure of a restoration and deep caries often lead to pulpal inflammation. In such cases where there is a low remaining dentin thickness, the vitality of the pulp is threatened and often necessitates costly root canal therapy or extraction. Pulp-capping techniques may be employed in an attempt to avoid this by allowing the pulp to recover and by supporting tertiary dentin formation in the proximity of a restoration [3, 4]. Unfortunately, pulp-capping techniques—particularly direct pulp-capping—generally have poor success rates. This is especially true in situations where the pulpal health has deteriorated to the degree that the pain caused by the decay leads the patient to seek treatment [5–7]. Pulp-capping also presents many challenges, foremost among them successful disinfection of the pulp, attenuation of pulpitis and, significantly, facilitation of dentin production at the material-dentin interface that will result in a well-sealed restoration [8, 9]. This last challenge is particularly important as it prevents microleakage of microorganisms, which drives the formation of secondary caries and causes continued irritation of the pulpal tissues. The solution to these problems may lie in the development of better pulp-capping materials that address the challenges inherent to the technique.

The ideal pulp-capping cement should be easy to use and will prevent root canals by increasing the success rates of these procedures. From a clinical perspective, the material should have an optimal and adjustable working time (the time that elapses between mixing the cement and the moment it can no longer be easily manipulated), and a reasonably rapid setting time (the period of time for the cement to reach a final, hardened state). The material should be relatively fast setting after this adequate working time. These properties should be adjustable to match a given patient and procedure. In regards to desirable properties, the cement should be comprised of biocompatible components, maintain a sufficient seal after placement to mitigate infection, and display good chemical durability over time [10].

As a pulp-capping cement, calcium hydroxide paste (CaOH) has long been considered state-of-the-art, due to its exceptional workability and fast setting times. [11, 12]. However, two aspects of this material that are in need of improvement are its sealing ability and long-term durability [10], as CaOH pastes have a poor sealing ability and do not have any inherent adhesive properties [13, 14]. These cements fail to provide permanent protection to the pulp, due to a tendency for dissolution [15]. In vitro, CaOH paste compositions have been shown to exhibit "tunnel defects," (cylindrical tunnels, >10μm in diameter), which may lead to bacterial leakages and eventual need for retreatment [16, 17].

To improve upon the issues with sealing and physical integrity after placement, mineral trioxide aggregate (MTA) was created and is increasingly considered the best available pulp-capping material. MTA is less soluble than CaOH pastes. It also has the advantage of enhanced sealing ability due to its expansion during setting [18, 19]. MTA has been found to mature into a calcium-deficient hydroxyapatite in phosphate containing body fluids [20–23]. While traditional MTA has a setting time of 2 to 4 h [24], compositions can be adjusted and resins can be added to make the cement set within 15 min [18]. Despite the widespread use of both MTA and CaOH pastes, both are problematic for user manipulation and placement [25]. Both materials are highly technique sensitive. In addition, the resins present in most modern MTA and CaOH paste formulations have been shown to increase the cytotoxicity of the material to pulp tissue [26]. Neither CaOH paste nor MTA meet the criterion of an ideal pulp-capping cement.

This study investigated a new material for endodontics inspired by commercial construction materials: a blend of sodium metasilicate (NaSi) and calcium phosphate (CaP) glasses. NaSi, also known as "water glass" or "invert glass," possesses a highly water-soluble network that is known to decrease setting time and increase final hardened strength when added to concrete [27, 28]. The NaSi was mixed with CaP in several ratios to create a pulp-capping cement with the short setting times and workability of CaOH pastes combined with the sealing ability and durability of MTA. The cement has a completely inorganic formulation, the components of which are similar to those of bioglass, the biocompatibility of which has been widely studied [29–31]. Its working and setting times, phase maturation in a phosphate buffered saline solution, and sealing ability were investigated. This material has the potential to become a new state-of-the-art formulation for pulp-capping applications.

2 Materials and methods

2.1 Glass fabrication

The sodium metasilicate (NaSi) glass was made by melting a sodium bicarbonate (Alfa-Aesar, Ward Hill, MA, USA) with silica (SiO_2) powder (Alfa-Aesar, Ward Hill, MA, USA) at 1100 °C for 1 h. A composition of 50 mol% Na_2O—50 mol% SiO_2 was selected for its proximity to the maximum solubility of sodium in the network [32]. The

calcium phosphate (CaP) glass was synthesized by melting monocalcium phosphate monohydrate [$Ca(H_2PO_4)_2{\cdot}H_2O$] powder (Alfa-Aesar, Ward Hill, MA, USA) at 1100 °C for 1 h. Monocalcium phosphate monohydrate was selected for the glass forming ability reported at Ca/P molar ratios near 1/2, as well as ease of processing. Melts were quenched on a stainless-steel plate and the resulting glass was ground into frit using an A-11-B-S001 grinder (IKA, Staufen, Germany). Granules were sieved to a particle size distribution between 106 and 150 µm using 3" diameter test sieves (Endecotts, London, UK). The results of this process were granules of NaSi and CaP glasses.

2.2 Glass characterization

Granule morphology was examined using scanning electron microscopy (SEM—Hitachi S-4800, Chiyoda, Tokyo, Japan) at an accelerating voltage of 5 kV, and the crystallinity was evaluated through powder X-ray diffraction (XRD—MiniFlex™, Rigaku, The Woodlands, TX, USA) with a scan rate of $0.5°2\theta\,s^{-1}$ and a step size of $0.05°2\theta$. The molecular structure of the glass-based cements was examined using attenuated total reflectance Fourier transform infrared spectroscopy (ATR-FTIR—Nicolet S50 FT-IR, Thermo Scientific, Waltham, MA, USA) with a diamond crystal. A background was collected less than 1 min before the data from each sample was collected in order to increase the signal-to-noise ratio and avoid drift in the data from interaction with CO_2.

2.3 Setting reaction

Cements were prepared for setting measurements by mechanically mixing different masses of NaSi and CaP powders (Table 1). Deionized (DI) water was then added to initiate the setting reaction. A powder-to-liquid (P/L) ratio of $2.5\,g\,mL^{-1}$ was chosen for all testing as it produced pastes that were easily manipulated while holding their shape without slumping under their own weight. The material was then mixed with a spatula for 30 s, allowing heat released during setting to dissipate.

Table 1 Chemical compositions of pulp-capping materials examined in this study: 25NaSi, 33NaSi, and 50 NaSi

Name	Composition
25NaSi	25 wt% NaSi[a]
	75 wt% CaP[b]
33NaSi	33 wt% NaSi
	67 wt% CaP
50NaSi	50 wt% NaSi
	50 wt% CaP

[a]NaSi glasses prepared at 50 mol% Na_2O—50 mol% SiO_2

[b]CaP glasses prepared at 33 mol% CaO—67 mol% P_2O_5

A procedure for determining the working and setting time of the cements was adapted from ISO 9917-1:2017 for the testing of water-based dental cements [33]. The standard calls for a rectangular, room-temperature aluminum mold placed on a piece of clean aluminum foil and filled to a level surface with mixed cement. Sixty seconds after the end of mixing, the assembly—comprising mold, foil, and cement specimen—is placed in an incubated cabinet (VWR Personal Low Temperature Incubator, VWR, Radnor, PA, USA) conditioned to 37 °C. Ninety seconds after the end of mixing, the working time indenter—a needle with a mass of 130 g and a flat end diameter of 2 mm—is carefully lowered vertically onto the surface of the cement and allowed to remain there for 5 s, repeating the indentations at 3 min intervals until the needle fails to make a complete circular indentation in the cement when viewed using ×2 magnification. The setting-time indenter, with a mass of 400 g and a flat end diameter of 1 mm, is similarly used thereafter at 3-min intervals. Setting time is recorded when the needle is unable to make a complete circular indentation in the surface of the sample. An initial trial was carried out as described above to determine the approximate working and setting times. The working time and setting time were then tested on two separate samples, starting the indentations at 90 s before the approximate working and settings times determined from the initial trial, making indentations at 30 s intervals in order to increase the temporal resolution of the measurements.

The working and setting times were recorded as the time elapsed between the end of mixing and the time when the needle failed to make a complete circular indentation in the cement. The experiments were carried out a total of three times. Trials were performed separately by different individuals to reduce measurement bias. Two one-way ANOVA tests were carried out for both working and setting times using JMP Pro 14 statistical analysis software to test for differences between the behavior of different compositions. These were performed using a significance level of $\alpha = 0.05$. A Student's t-test at the same significance level was also carried out on each pair of compositions.

The temperature of each cement composition was measured starting immediately (<5 s) after addition of water using an infrared thermometer (Fisherbrand Traceable Infrared Thermometer Gun, Fisher Scientific, Hampton, NH). The thermometer was calibrated and tested by the manufacturer and has a maximum uncertainty of 1.1 °C. The maximum temperature was recorded as the maximum temperature reached in the first 5 min after mixing to assess how the endothermic nature of the cements varies with composition. After setting, samples were kept in a sealed

cabinet to dry at 37 °C for 24 h. Samples were then examined using SEM and ATR-FTIR.

2.4 Sealing ability measurement

The method that was applied in this study for testing sealing ability of a dental cement was adapted from a method previously used by Aqrabawi and involves placing a sample of pulp-capping cement in methylene blue dye for a predefined period and measuring the depth of dye penetration [34]. In this study, right circular cylindrical samples of cement were prepared. Three samples of each composition of NaSi-CaP cement were mixed and allowed to set in cylindrical plastic molds. After setting for 24 h, each cylinder was lightly ground to a diameter of 9 mm and a height of 11 mm. The sides and one face of each disk were covered with two coats of clear acrylic varnish in order to isolate one surface through which dye penetration could be observed. The samples were immersed in a 0.5% solution of methylene blue dye (Beantown Chemical, Hudson, NH, USA) for 24 h at 37 °C, at which point they were sectioned with a low-speed circular saw at an angle perpendicular to the face of the cylinder. The depth of dye penetration and physical condition of the samples was evaluated using a stereomicroscope at ×3 magnification. The experiment was repeated a total of three times.

2.5 Cement incubation

To examine in vitro phase maturation behavior, a sample of each NaSi-CaP cement composition was mixed and allowed to set for 24 h before being placed in 2 mL of a phosphate buffered saline (PBS) solution with a pH of 7.2. Cements were incubated for 7 days at 37 °C. The samples were then removed, dried, and the microstructure was observed using SEM. Samples were then crushed into a fine powder and examined using XRD and ATR-FTIR.

3 Results

3.1 Setting reaction

The NaSi and CaP glass granules (Fig. 1a, b) have similar morphologies and particle sizes. ATR-FTIR spectra of the mixed glass compositions display only characteristic peaks from the parent glasses. The gradual appearance of the characteristic peaks from one phase as the other decreases indicates that the glasses are only physically mixed and not chemically reacting in ambient conditions (Fig. 1c). The band present in all NaSi-containing compositions at roughly 1150 cm^{-1} which ranges from 1100 to 1300 cm^{-1} is indicative of Si-O stretching vibrations and can be attributed to the

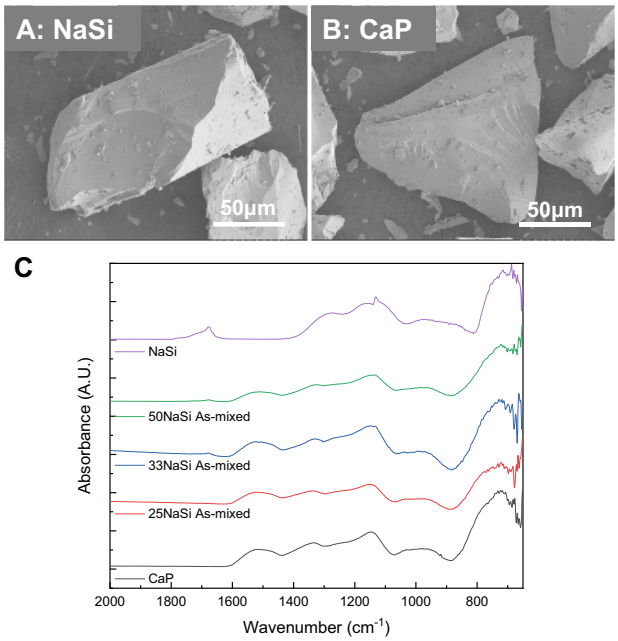

Fig. 1 The irregularly shaped NaSi granules (**a**) and CaP granules (**b**) possess similar morphologies prior to mixing. FTIR on the NaSi and CaP granules before setting (**c**). The glass mixtures show characteristic peaks from both pure glasses, indicating only physical interactions upon mixing. The band at around 1500 cm^{-1} is indicative of CO_2 adsorbed to phosphate particles

Table 2 FTIR absorption band assignments used throughout this study

Wavenumber (cm^{-1})	FTIR band assignments
630, 600, 560, 520	Asymmetric bending of PO_4
900	Asymmetric stretching of PO_4
1080	Si-O-Si stretching
1100–1200	Si-O stretching
1250	Asymmetric stretching of O-P-O
1340	Stretching of P=O
1650	OH water-adsorbed bending
3400–3420	Water-adsorbed deformation
3570	O-H stretching

disconnected silica tetrahedra present in NaSi (Table 2). A band centered at 1340 cm^{-1} is assigned to the stretching of P = O units within phosphate tetrahedra. Another band at 1500 cm^{-1} is due to adsorbed atmospheric CO_2.

Mean working and setting times of each composition, as well as the average maximum temperature reached during setting are shown in Fig. 2. Exothermic reactions occurred upon mixing the NaSi-CaP cements with water. The exothermic effect is greater for cements with higher NaSi content due to the higher reactivity with water. In each sample, this heat lasted a short time and dissipated before the time at which the material would be applied to the

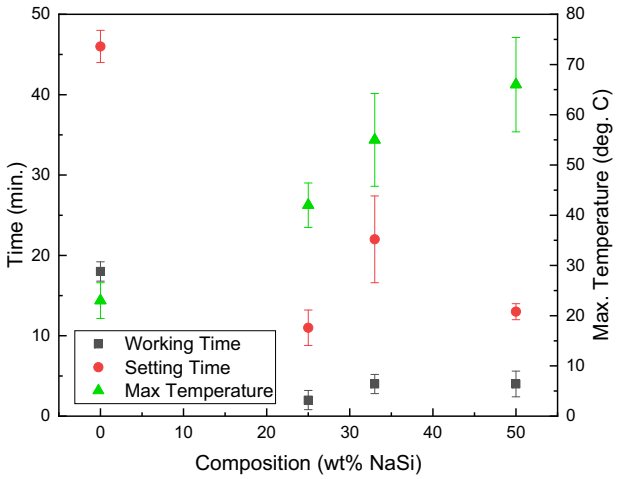

Fig. 2 Working and setting times for NaSi-CaP cements, as well as average maximum temperature reached during setting. The values represent the mean ± the uncertainty of N = 3 measurements. Working time is longest for 0 wt% NaSi but decreases to under 5 min in samples with 25–50 wt% NaSi. Setting time appears to decrease linearly as the NaSi concentration increases, with the exception of the 25 wt% NaSi samples, which deviates significantly. The maximum temperature generally increases as the NaSi concentration increases

patient. While temperatures are high initially, the mixtures return to below 30 °C within 60 s after the addition of water.

NaSi concentrations in the range of 25–50 wt% provided cements with desirable consistencies: a smooth putty that could be formed into a shape and would not slump under its own weight. Note that preliminary testing demonstrated that compositions with greater than 50 wt% NaSi had the consistency of wet sand and would not hold their shape. The cements slumped after mixing and never reached conditions for working or setting time within a meaningful amount of time (<24 h).

The mean working time of the pure CaP was significantly higher than those of the glass mixtures. The CaP had a working time of 18 ± 1.2 min. The addition of the NaSi drastically reduced the working time to between 2–5 min. No statistical difference was observed in the working time of the glass mixtures.

While no statistically significant variation was seen in working time, setting times differed with NaSi concentration. The setting time of the CaP was 46 ± 2.0 min. 25NaSi had a setting time of 11 ± 2.2 min, which lacks statistically significant differences when compared to the setting time of 50NaSi, which had a value of 13 ± 1.0 min. The setting time of 33NaSi, which was statistically significantly higher than the other two glass mixtures, was 22 ± 5.4 min. While the mean *working times* of 25NaSi, 33NaSi, and 50NaSi lack statistically significant differences, the mean *setting time* of 33NaSi is statistically significantly higher than the other two compositions. The results showed that working times remain constant in the range of 25 to 50 wt% NaSi, while setting time varies in a nonlinear manner.

SEM examination of the glass mixtures after setting provided insight into the working and setting behavior (Fig. 3). For the CaP (Fig. 3a), individual granules are still visible that show slight degradation. This observation correlates well to the subjective properties of the bulk sample observed during handling in which the sample readily crumbles as particles appear to be only loosely held together. Pure NaSi has the exact opposite appearance (Fig. 3e) in that all the granules have completely degraded into a hydrated matrix with a relatively smooth, solid surface. This observation explains the behavior of the bulk sample, which never fully sets. Of note, these samples were observed to remain pliable even after 1 month in the incubation cabinet at 37 °C.

The cements that were a mixture of CaP and NaSi had an appearance similar to the parent materials; the 25NaSi was largely granular while 50NaSi appears similar to the pure NaSi but with a slightly rougher surface. The 33NaSi had a blend of CaP granules suspended in hydrated matrix of NaSi. These images also correlate to the behavior of the bulk samples. Pure CaP has a chalky texture after setting and crumbles easily during handling. The addition of NaSi appears to make the set samples more physically robust, as particles are not shed from the surfaces of these samples during handling and they cannot be easily crushed in the hand. Set NaSi-CaP cements are white in color and visually homogeneous.

The ATR-FTIR spectra after setting (Fig. 4) showed that chemical changes in the cements occurred during setting. The large band indicative of PO_4 asymmetric stretching vibrations at 900 cm^{-1}, present in all set samples, was not present prior to setting (Fig. 1c). The large band that is indicative of O-P-O stretching vibrations between tetrahedra at roughly 1250 cm^{-1} present in all three glasses prior to setting (Fig. 1c) largely disappears when the samples are set with the effect being most pronounced in the 25NaSi sample. The band is reduced to a shoulder during/after the setting process with slightly different behavior depending on the NaSi concentration of the glass mixture. The relative size reduction of this peak is indicative that corrosion of CaP particles occurred during setting. The 33NaSi samples show the remnant of this band with moderate absorption intensity, though having its peak pushed to a slightly lower wavenumber. In the 25NaSi composition, a band located at 1080 cm^{-1}, is indicative of Si-O-Si stretching vibrations associated with interconnected silica tetrahedra. In 33NaSi and 50NaSI, this peak is shifted to a slightly higher wavenumber (1100–1150 cm^{-1}), indicating Si-O stretching vibrations associated with a larger amount of disconnected tetrahedra. These results show that cement samples set as Si-O-Si linkages are formed in the hydrated matrix and as CaP particles begin to corrode.

X-ray diffraction of set samples (Fig. 5) did not show the formation of crystalline phases during setting. Bulk

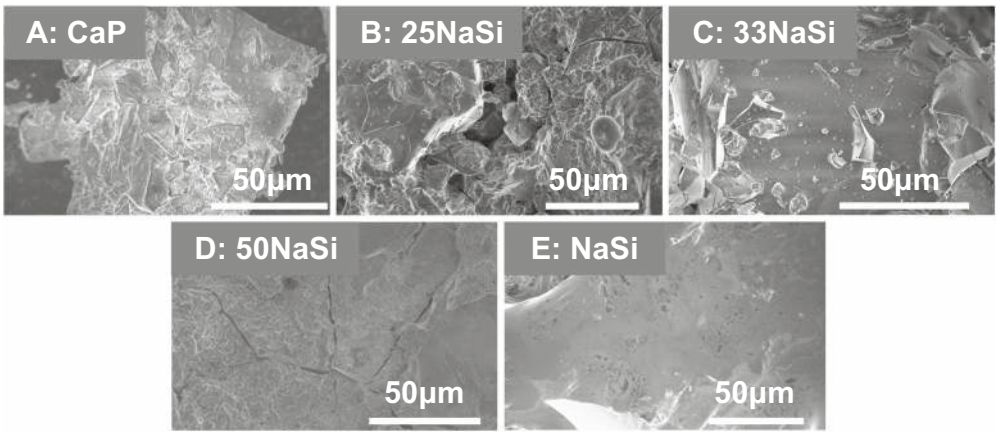

Fig. 3 NaSi-CaP cement compositions 24 h after setting. CaP (**a**) 25NaSi (**b**), 33NaSi (**c**), 50NaSi (**d**), NaSi (**e**). As the amount of NaSi in a sample increases, the surface of the set sample appears to be smoother due to the hydrated matrix which is formed by the NaSi and coats the CaP granules. The cracking seen on the surface of the sample in (**d**) occurred during drying of the sample for imaging

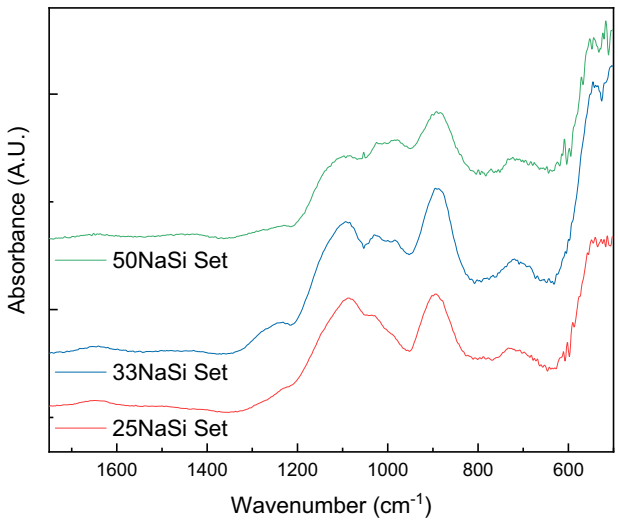

Fig. 4 All samples after setting were X-ray amorphous; however, ATR-FTIR on set samples showed that chemical reactions were taking place. Pure CaP and NaSi samples were not included as they did not set. 33NaSi shows a band at around 1250 cm^{-1} that is only faintly present in the other two compositions. 33NaSi and 50NaSi show a pair of peaks centered at around 1000 cm^{-1}, whereas the 25NaSi exhibits the lower wavenumber of the two peaks (980 cm^{-1}) only as a faint shoulder

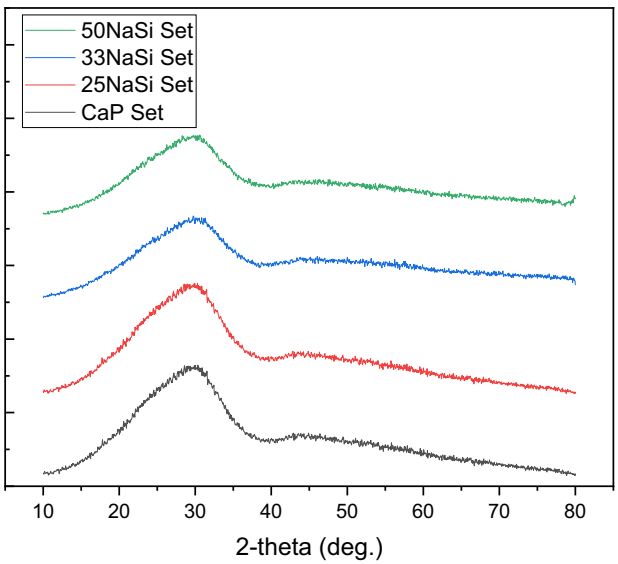

Fig. 5 After 24 h of setting, X-ray diffraction patters are featureless, characteristic of amorphous phases. No detectable crystalline peaks are present

crystallization of samples during setting reaction is not observed.

3.2 Sealing ability

The sealing capabilities of the various cements varied with NaSi concentration as shown in Fig. 6. Pure CaP is unable to retain structural integrity after 24 h in dye solution (Fig. 6a). This behavior is a result of the minimal corrosion experienced during setting, leaving the sample as an agglomeration of loosely bound granules that fall apart when immersed in the dye solution. The addition of NaSi in the 25NaSi and 33NaSi samples keeps the samples structurally sound in the solution; however, the hygroscopic nature of the NaSi allows for water to diffuse through the cement (Fig. 6b, c). The absorption is more pronounced in the 50NaSi, causing the swelling and loss of structure, resulting in the delamination from the protective coating of varnish. The results of this experiment show that the addition of NaSi within certain compositional ranges improves the sealing ability of CaP glass.

3.3 In vitro phase maturation

Upon 1 week of incubation in PBS, all compositions showed peaks indicative of crystallization, with amorphous regions still evident between 20–40° 2θ (Fig. 7). Crystalline

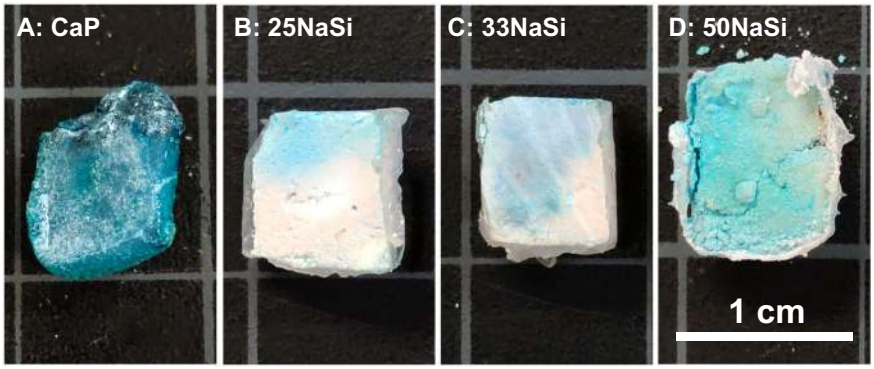

Fig. 6 After 24 h in dye solution, dye penetration and sample condition vary with NaSi concentration. Pure CaP (**a**) is saturated with dye causing a loss of mechanical strength. 25NaSi (**b**) and 33NaSi (**c**) are structurally sound after 24 h in dye solution and show an increasing dye penetration depth with increasing NaSi concentration. 50NaSi samples have swollen to a larger size and have generally lost their structural integrity

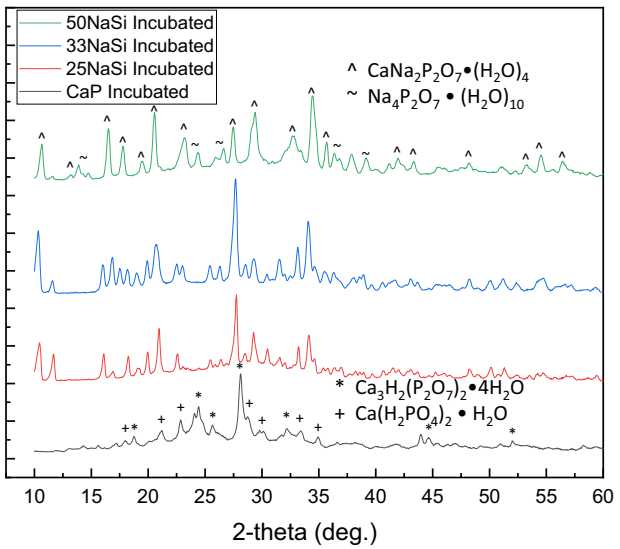

Fig. 7 X-ray diffraction patterns after 1 week of incubation in PBS at 37 °C. Phases present in CaP were identified as hydrated calcium phosphates. 25NaSi was determined to match brushite as its dominant phase. Phases matching 33NaSi and 50NaSi were shown to incorporate more sodium, including phases such as sodium phosphate hydrate and canaphite ($CaNa_2P_2O_7·(H_2O)_4$). Data sets with more than one identified phase are marked with symbols to show which peaks can be attributed to which phase

phases were identified using the International Centre for Diffraction Data (ICDD) database. Phases present in each composition are listed in Table 3.

Both phases identified in CaP samples are hydrated calcium phosphates. The first, $Ca(H_2PO_4)_2•H_2O$, is monocalcium phosphate monohydrate and has the same stoichiometry as the precursor powder used to create the glass. The second is a tricalcium phosphate phase. Brushite, which is a hydrated calcium phosphate phase, was found to be the apparent dominant phase present in the 25NaSi sample. Based on the phases identified in spectral data for 33NaSi and 50NaSi, these samples appear to have incorporated

Table 3 Phases identified from the ICDD database through X-ray diffraction of incubated samples

Sample name	Identified phases
CaP	$Ca(H_2PO_4)_2•H_2O$
	$Ca_3H_2(P_2O_7)_2•4H2O$
25NaSi	Brushite, $CaHPO•2H_2O$
33NaSi	Canaphite, $CaNa_2P_2O_7•(H_2O)_4$
50NaSi	Canaphite, $CaNa_2P_2O_7•(H_2O)_4$
	$Na_4P_2O_7•(H_2O)_{10}$

sodium into their structures to form canaphite, with 50NaSi also showing the formation of a hydrated sodium phosphate.

The ATR-FTIR of the incubated samples (Fig. 8) shows a large degree of hydration, with prominent bands appearing at roughly 1650 cm^{-1} and the region between 3000 and 3600 cm^{-1}, providing supporting evidence of the hydrated calcium phosphate phases obtained from the XRD analysis. The 25NaSi sample, which was primarily composed of brushite, contains the lowest degree of hydration. The 50NaSi sample shows the most extensive degree of hydration, which corresponds to the presence of the canaphite, $CaNa_2P_2O7•(H_2O)$, and hydrated sodium phosphate, $Na_4P_2O_7•(H_2O)_{10}$. The HPO_4 absorption band, which is a broad, low-intensity band spanning the region from 1800–2500 cm^{-1} has become the most prominent and well-resolved in the 50NaSi incubated sample. The rod-like morphology of the crystals observed in the 50NaSi composition using SEM (Fig. 9d) also differs from the morphologies observed in the other compositions (Fig. 9a, c), which show needle-like and plate-like crystals.

In the cation region of the ATR-FTIR data from roughly 500 to 1800 cm^{-1}, significant molecular bonding changes may be observed in comparing the plots of the mixed, set,

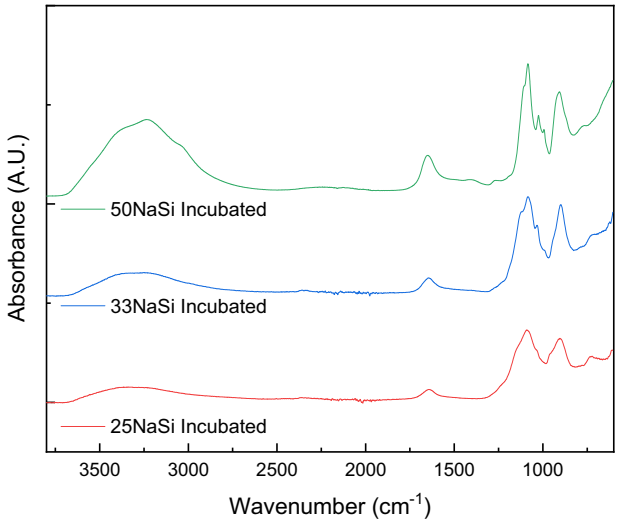

Fig. 8 ATR-FTIR shows a broad band indicative of hydration centered at around 3200 cm^{-1} in all four samples, with the relative intensity of this band being largest in the 50NaSi Sample. Un-mixed CaP shows peaks in the range of 1250–1750 cm^{-1} which are not present in the mixed NaSi-CaP compositions

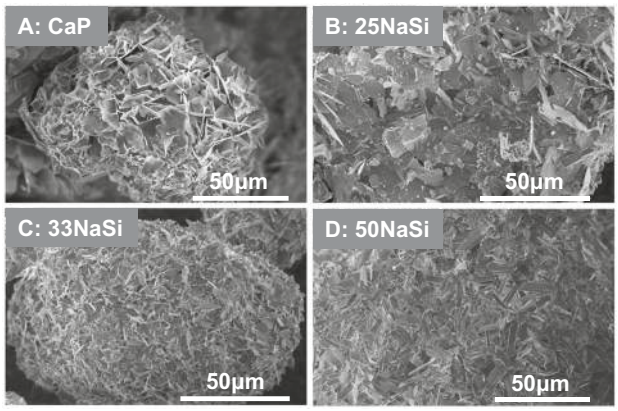

Fig. 9 NaSi-CaP compositions after one week of incubation in phosphate buffered saline solution. CaP (**a**), 25Na (**b**), 33Na (**c**), 50Na (**d**). Unmixed NaSi dissolves in PBS at incubation temperatures and is therefore not shown. Crystallization can be observed in micrographs from all compositions containing CaP, including un-mixed CaP (**a**). The morphologies of crystals in mixed NaSi-CaP samples vary with NaSi loading. While pure CaP, 25Na, and 33Na all show needle-like and plate-like crystals (**a**-**c**). 50Na shows larger, rod-like crystals (**d**)

and incubated samples. The overlaid spectra are shown in Fig. 10.

For the SiO_2 region, the band with the highest intensity is near 900 cm^{-1}, while the next highest is centered around 1075 cm^{-1}. The band centered at 900 cm^{-1} is observed to sharpen in width and increase in height, which corresponds to the asymmetric stretching vibration of P-O associated with the increasing number of PO4 units, possibly forming at the expense of SiO4 units. The formation of crystalline silicates has not been observed in either the XRD (Fig. 7) or the ATR-FTIR data. The development of the crystalline PO4 units are evident at several wavenumber ranges in the ATR-FTIR spectra, while the Si is most likely continuing to be bound in whatever X-ray amorphous (glassy) regions remain in the incubated samples. The Si-O features can often be convolved with P-O features in the ATR-FTIR spectra, and it would appear that the vibrations due to the forming crystalline arrangements of PO4 are of more intense absorption than those for the remaining (and decreasing amount of) silicate glass regions of the samples. Evidence of this is observed in the peak shift from silica attributed peaks in the set samples to phosphate attributed peaks in the incubated samples. After incubation, the band at 1080 cm^{-1} is shifted to 1090 cm^{-1} with the increasing presence of phosphate groups.

Another characteristic vibration of the forming phosphate crystals is the asymmetric bending vibration of PO4 at around 600 cm^{-1} in the 25NaSi set and incubated samples, 560 cm^{-1} in the 33NaSi set sample, and at roughly 550–560 cm^{-1} and 605–630 cm^{-1} in the 33NaSi incubated sample. 33NaSi is the only incubated sample in which this division of sites is seen. The 50NaSi set sample shows this asymmetric bending vibration of PO4 being in two sites shifted to about 570 and 610 cm^{-1} relative to the original position in the 25NaSi pre-setting. For the 50NaSi incubated sample, it appears that absorption due to asymmetric bending has become broader and more all-encompassing within the region between 500 and 700 cm^{-1}, appearing as a prominent shoulder on a band now peaking at around 520 cm^{-1}.

4 Discussion

The NaSi-CaP cements used in this study had working times in the range of 2–5 min and setting times between 10–25 min (Fig. 2). The reported working time for a CaOH pulp-capping cement (Dycal) is 0.5 min with a setting time of 2–3 min [35], while MTA (MTA Fillapex) is reported to have a working time of 23 min and a setting time of 130 min [36]. Modern formulations of both MTA and CaOH rely on organic resins for catalysis of setting reactions and improved consistency. These components have been shown to increase cytotoxicity to pulp cells [26]. The NaSi-CaP cements in the present study have working and setting times similar to and in some cases quicker than clinically used materials and do not contain organic resins. Instead, these cements make use of the natural corrosion properties of the component glasses.

In the NaSi glass, there is a 1:1 molar ratio between Na_2O and SiO_2, causing the typically highly connected, covalently bonded Si-O network to form isolated SiO_4 tetrahedra. Bonding in these glasses occurs through Van der

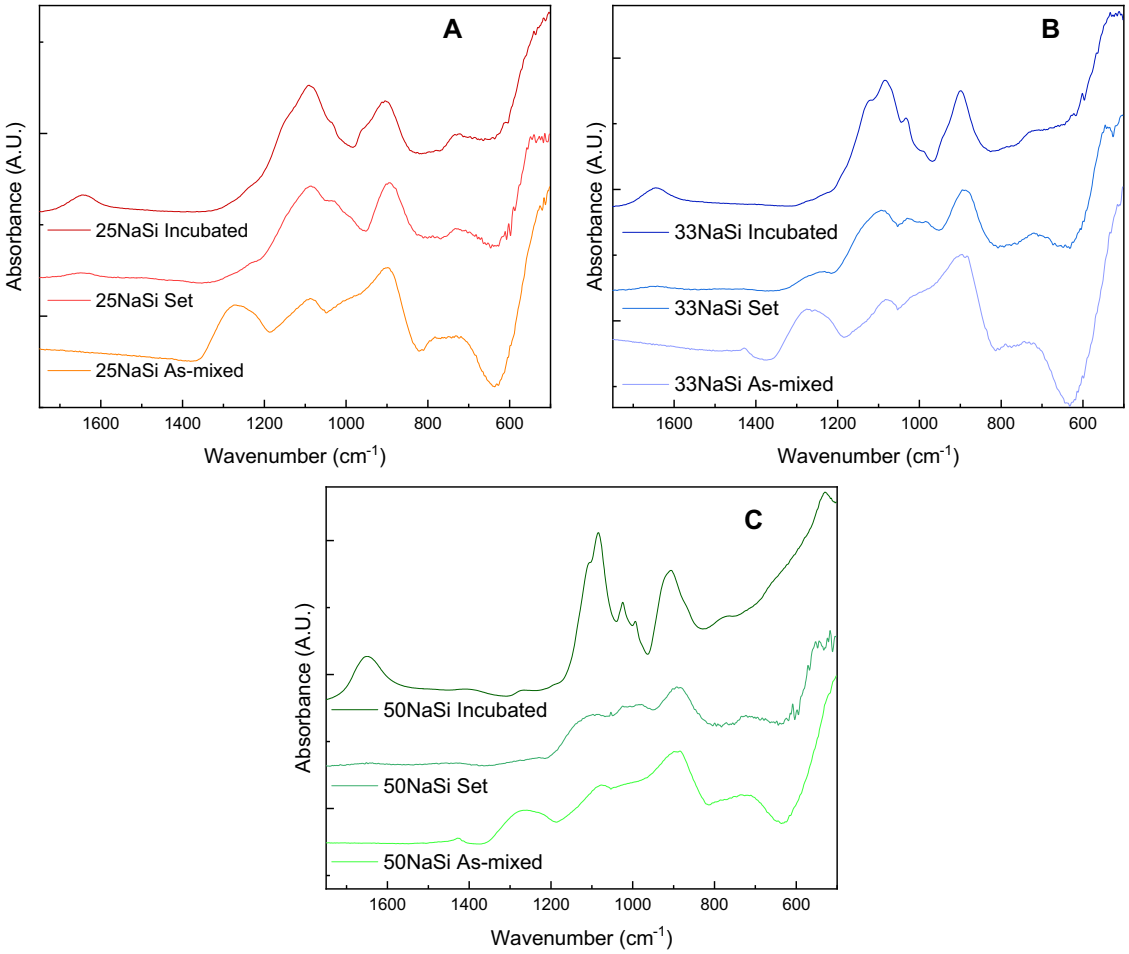

Fig. 10 FTIR of 25NaSi (**a**), 33NaSi (**b**), and 50NaSi (**c**) pre-setting, 24 h after setting (set), and after 1 week of incubation in PBS (incubated)

Waals forces between the sodium ions, which easily corrode upon exposure to water to form a hydrated matrix [28]. CaP glasses are also susceptible to aqueous attack, although to a much lesser extent than the NaSi. In this case, the phosphate glasses are composed of a cross-linked network of tetrahedra with a non-bridging oxygen at one vertex of each PO_4 group. The introduction of calcium ions increases the quantity of non-bridging oxygens, depolymerizing the network into linear chain structures. These long chains shorten as modifier content increases, reducing the network's durability. The initial stages of aqueous reactions result in the leaching of calcium from the surface of the glass to create a P_2O_5-rich surface layer [37].

The working and setting times of the NaSi-CaP cements are dictated by the physical structure provided by the slow-corroding CaP particles and the hydrated matrix formed by the NaSi that binds them together. For CaP, no temperature change was observed upon mixing with DI water and the set samples easily crumbled during handling. Investigation of the set sample with SEM showed that the individual particles were still visible with minimal surface corrosion (Fig. 3a). Therefore, the change in physical properties of the cement is attributed to hydration, swelling, and subsequent physical interlocking of the particles. The addition of NaSi in the range of 25 to 50 wt% drastically decreased the working and setting time due to the formation of the hydrated silica matrix and the physical interlocking of CaP particles. However, when NaSi content is >75 wt% the cements were never observed to set because they do not have the structure provided by the slow-corroding particles of CaP.

The linear trend observed in setting time with varying amounts of NaSi was not followed by the 25NaSi cement composition (Fig. 2). 25NaSi appears to deviate from the general trend with a much lower setting time than either the pure CaP or 33NaSi compositions. The low setting time of 25NaSi appears to be due to the interactions between two factors: temperature and hydrated matrix formation. Generally, decreases in setting time and increases in temperature during setting correlate well with one another in that the

corrosion of CaP is expected to be faster at higher temperatures. Though higher temperatures were reached in the 33NaSi and 50NaSi samples, the hydrated matrix formed by the dissolved NaSi quickly coated the CaP particles and appears to have inhibited their corrosion [38]. Conversely, the NaSi present in the 25NaSi sample caused a sufficient increase in temperature to begin the corrosion of the CaP particles but did not form enough of a hydrated matrix to interfere with the reaction. Additionally, it was observed that vibrations indicative of Si-O-Si linkages were more intense in the 25NaSi composition (Fig. 4). This shows that in the 25NaSi samples, the lower number of sodium ions interact preferentially with the CaP before the SiO4 tetrahedra. Unimpeded by the sodium, more of the SiO4 tetrahedra can interact to form Si-O-Si bonds, leading to a quicker setting time.

The chemical reaction responsible for setting continues to occur as mature phases are formed during the incubation of these cements. It is proposed that this process may be expressed by the following reaction:

$$\mathrm{Na_2O \cdot SiO_2 + CaO \cdot P_2O_5 + nH_2O \rightarrow CaO \cdot \mathit{m}P_2O_{5\,Hydrate} + SiO_{2\,Hydrate} + (Ca, Na_2)O \cdot \mathit{P}_2O_{5\,Hydrate}} \quad (1)$$

where m and n are constant moduli based on the relative amounts of CaO to P_2O_5 and H_2O respectively. The products of this reaction are hydrated SiO_2, hydrated calcium phosphates, and hydrated calcium phosphates with a portion of the calcium ions substituted for pairs of sodium ions. In addition to the breakdown and release of sodium ions from the NaSi structure, the formation of products in the above reaction also produces heat [39]. The shift in the ATR-FTIR peak, which indicates the symmetric bending mode of PO_4 vibration, from 1075 cm^{-1} in the set samples (Fig. 4) to 1085 cm^{-1} after incubation (Fig. 8) indicates that sodium is taking the place of some calcium in the products.

25NaSi samples formed a crystalline brushite phase after one week of incubation in PBS. Brushite is a known bioactive and bio-resorbable calcium phosphate phase and is a precursor for hydroxyapatite formation in the body [40]. It is of particular note that brushite did not form in the pure CaP, 33NaSi or 50NaSi samples. Instead, these compositions showed phases indicative of sodium incorporation and substitution: canaphite and hydrated sodium phosphates. Additional evidence of sodium incorporation into the calcium phosphate structures is seen in the relative increase in size of the ATR-FTIR peak associated with the symmetric bending mode of PO_4 vibration located at 1085 cm^{-1} (Fig. 10). This peak has the greatest relative size in the incubated 50NaSi samples, which correlates with the presence of sodium phosphate phases found using XRD present only in that composition.

NaSi on its own is highly hygroscopic and therefore allows for the diffusion of water. As NaSi undergoes hydrolysis and sodium ions are released during setting, SiO4 tetrahedra with non-bridging oxygens disassociate from each other to form hydrated silicates such as silicic acid [38]. After setting, the cements no longer exhibited the same degree of hygroscopicity because the majority of the silica had already hydrated as evidenced by the broad, low absorption band attributed to OH groups at 1650 cm^{-1} (Fig. 4). The resulting hydrated species acted as binders to hold the particles of CaP together. In pure CaP samples, liquid moved through the entire sample and degraded it until the form slumped. The 50NaSi swelled and subsequently degraded, forming cracks and porosity which allowed liquid to penetrate through the bulk sample [38].

While dye penetration is not a direct corollary for bacterial leakage [41], it can serve as a conservative preliminary analog to screen candidate endodontic materials. When a pulp-capping material does not allow penetration of small dye molecules, it has the potential to prevent leakage of larger substances such as bacteria and their byproducts [34, 42–44]. In the context of this study, dye penetration is used as a means of exploring the effects of NaSi content on the sealing behavior and physical robustness of these glass-derived cements.

The ability of water to diffuse through the 25NaSi and 33NaSi samples without a corresponding compromise in the structural cohesiveness of the material may be beneficial in pulp-capping. Diffusion could allow blood components and soluble bioactive factors from the dentin pulp complex to infiltrate the cement. Such infiltration should also enhance the bioactivity of the material. Moreover, this cement is expected to be placed under a restoration and is not intended as a direct restorative material. Therefore, water permeability is not likely to enhance microleakage from the oral cavity around the margins of the restoration.

5 Conclusion

Like MTA, the NaSi-CaP pulp-capping material investigated in the present study was inspired by materials used in the construction industry. NaSi and CaP glasses can be combined to form a material which has favorable setting properties, can form an effective seal, and produces mature phases suitable for pulp capping. The working and setting times can be adjusted by varying the relative amounts of NaSi and CaP due to the varying interactions between these two glasses. NaSi-CaP cements were shown to mature into appropriate phases in the presence of PBS. The material forms a structural seal while allowing for the diffusion of liquid. This material achieves properties which are like

those of clinically used materials while having a relatively simple inorganic composition.

Acknowledgements This work was funded in part by the National Science Foundation REU under the parent grant CMMI #1660979. It is also supported by Dawn and Roger Crus, a USTAR Science and Technology Initiation grant, and a grant from the Undergraduate Research Opportunities Program at the University of Utah.

Compliance with ethical standards

Conflict of interest The authors declare that they have no conflict of interest.

Publisher's note Springer Nature remains neutral with regard to jurisdictional claims in published maps and institutional affiliations.

References

1. Jin L, Lamster I, Greenspan J, Pitts N, Scully C, Warnakulasuriya S. Global burden of oral diseases: emerging concepts, management and interplay with systemic health. Oral Dis. 2016;22:609–19. https://doi.org/10.1111/odi.12428.
2. Dye B, Tan S, Smith V, Lewis B, Barker L, Thornton-Evans G. Trends in oral health status: United States, 1988-1994 and 1999-2004. Vital and health statistics series 11. Data Natl health Surv. 2007;248:1–92.
3. Rosa WLdOd, Silva TMd, Demarco FF, Piva E, Silva AFd. Could the application of bioactive molecules improve vital pulp therapy success? A systematic review. J Biomed Mater Res Part A. 2017;105:941–56. https://doi.org/10.1002/jbm.a.35968.
4. Schwendicke F, Stolpe M. Direct pulp capping after a carious exposure versus root canal treatment: a cost-effectiveness analysis. J Endod. 2014;40:1764–70.
5. Raedel M, Hartmann A, Bohm S, Konstantinidis I, Priess H, Walter M. Outcomes of direct pulp capping: Interrogating an insurance database. Int Endod J. 2016;49:1040–7. https://doi.org/10.1111/iej.12564.
6. Çalışkan M, Güneri P. Prognostic factors in direct pulp capping with mineral trioxide aggregate or calcium hydroxide: 2- to 6-year follow-up. Clin Oral Investig. 2017;2:357–67. https://doi.org/10.1007/s00784-016-1798-z.
7. Linu S, Lekshmi M, Varunkumar V, Joseph VS. Treatment outcome following direct pulp capping using bioceramic materials in mature permanent teeth with carious exposure: a pilot retrospective study. J Endod. 2017;43:1635–9. https://doi.org/10.1016/j.joen.2017.06.017.
8. Landuyt KV, Meerbeek BV. Restorative challenges and how to overcome them. In: Schwendicke F, editor. Management of deep carious lesions. New York City, NY, USA: Springer International Publishing; 2018. p. 71–91.
9. Smith A, Duncan H, Diogenes A, Simon S, Cooper P. Exploiting the bioactive properties of the dentin-pulp complex in regenerative endodontics. J Endod. 2016;42:47–56. https://doi.org/10.1016/j.joen.2015.10.019.
10. Rosa WLdOd, Silva TMd, Demarco FF, Piva E, Silva AFd. Current trends and future perspectives of dental pulp capping materials: a systematic review. J Biomed Mater Res Part B. 2018;106:1358–68.
11. Poggio C, Beltrami R, Colombo M, Ceci M, Dagna A, Chiesa M. In vitro antibacterial activity of different pulp capping materials. J Clin Exp Dent. 2015;7:e584–e8. https://doi.org/10.4317/jced.52401.
12. Mickenautsch S, Yengopal V, Banerjee A. Pulp response to resin-modified glass ionomer and calcium hydroxide cements in deep cavities: a quantitative systematic review. Dent Mater. 2010;26:761–70. https://doi.org/10.1016/j.dental.2010.03.021.
13. Hilton TJ. Keys to clinical success with pulp capping: a review of the literature. Operative Dent. 2009;34:615–25. https://doi.org/10.2341/09-132-0.
14. Yalçin M, Barutcigil Ç, Sisman R, Yavuz T, Oruçoglu H. Evaluation of the sealing ability of pulp capping agents against leakage on direct pulp capping with a computerized fluid filtration meter. J Restor Dent. 2014;2:46–50.
15. Gopika GJ, Ramarao S, Usha C, John BM, Vezhavendhan N. Histological evaluation of human pulp capped with light-cured calcium based cements: a randomized controlled clinical trial. Int J Sci Rep. 2017;3:120–7.
16. Kitasako Y, Ikeda M, Tagami J. Pulpal responses to bacterial contamination following dentin bridging beneath hard-setting calcium hydroxide and self-etching adhesive resin system. Dent Traumatol. 2008;24:201–6. https://doi.org/10.1111/j.1600-9657.2007.00517.x.
17. Nair PNR, Duncan HF, Pitt Ford TR, Luder HU. Histological, ultrastructural and quantitative investigations on the response of healthy human pulps to experimental capping with mineral trioxide aggregate: a randomized controlled trial. Int Endod J. 2007;0:071026203843001 https://doi.org/10.1111/j.1365-2591.2007.01329.x.
18. Tawil P, Duggan D, Galicia J. Mineral trioxide aggregate (MTA): Its history, composition, and clinical applications. Compend Contin Educ Dent. 2015;36:247–52.
19. Shenkin J, Wilson L. Mineral trioxide aggregate may be the most effective direct pulp capping material. J Evid-Based Dent Pract. 2019;19:183–5. https://doi.org/10.1016/j.jebdp.2019.05.003.
20. Chang S-W. Chemical characteristics of mineral trioxide aggregate and its hydration reaction. Restor Dent Endod. 2012;37:188–93.
21. Gandolfi MG, Siboni F, Botero T, Bossù M, Riccitiello F, Prati C. Calcium silicate and calcium hydroxide materials for pulp capping: bioninteractivity, porosity, solubility and bioactivity of current formulations. J Appl Biomater Fundamental Mater. 2015;13:43–60.
22. Malhotra N, Agarwal A, Mala K. Mineral trioxide aggreagate: a review of physical properties. Compend Contin Educ Dent. 2013;34:e25–32.
23. Tanomaru-Filho M, Morales V, Silva GFd, Bosso R, Reis JM, Duarte MAH, et al. Compressive strength and setting time of MTA and portland cement associated with different radiopacifying agents. Int Sci Res Notices. 2012;2012:898051.
24. Alex G. Direct and indirect pulp capping: a brief history, material innovations, and clinical case report. Compend Contin Educ Dent. 2018;39:182–189.
25. Ha WN, Kahler B, Walsh L. Clinical maniplation of mineral trioxide aggregate: lessons from the construction industry and their relevance to clinical practice. J Can Dent Assoc. 2015;81:f4.
26. Chen L, Suh BI. Cytotoxicity and biocompatibility of resin-free and resin-modified direct pulp capping materials: a state-of-the-art review. Dent Mater. 2017;36:1–7. https://doi.org/10.4012/dmj.2016-107.
27. Coppola L, Buoso A, Coffetti D, Kara P, Lorenzi S, D'Alessandro F. The effect of sodium silicate on the behaviour of shotcretes for tunnel lining. J Sci Res Rep. 2017;14:1–8. https://doi.org/10.9734/jsrr/2017/33641.
28. Song Z, Xue X, Li Y, Yang J, He Z, Shen S, et al. Experimental exploration of the waterproofing mechanism of inorganic sodium

silicate-based concrete sealers. Constr Build Mater. 2016;104:276–83. https://doi.org/10.1016/j.conbuildmat.2015.12.069.
29. Brandão SM, Schellini SA, Moraes AD, Padovani CR, Pellizzon CH, Peitl O, et al. Biocompatibility Analysis of Bioglass® 45S5 and Biosilicate® Implants in the Rabbit Eviscerated Socket. Orbit. 2012;31:143–9. https://doi.org/10.3109/01676830.2011.648798.
30. Krishnan V, Lakshmi T. Bioglass: a novel biocompatible innovation. J Adv Pharm Technol Res. 2013;4:78–83.
31. Wilson J, Pigott GH, Schoen FJ, Hench LL. Toxicology and biocompatibility of bioglasses. J Biomed Mater Res. 1981;15:805–17. https://doi.org/10.1002/jbm.820150605.
32. O'Donnell MD, Hill RG. Influence of strontium and the importance of glass chemistry and structure when designing bioactive glasses for bone regeneration. Acta Biomater. 2010;6:2382–5. https://doi.org/10.1016/j.actbio.2010.01.006.
33. ISO. Dentistry—Water-based cements—Part 1: Powder/liquid acid-base cements (Standard No. 9917-1). Switzerland. 2007. Retrieved from: http://iso.org.
34. Aqrabawi J. Sealing ability of amalgam, super EBA cement, and MTA when used as retrograde filling materials. Br Dent J. 2000;188:266–8. https://doi.org/10.1038/sj.bdj.4800450.
35. Dentsply International Inc. Dycal calcium hydroxide liner. York, PA: Dentsply Caulk; 2005.
36. MTA Fillapex. Angelus Indústria de Produtos Odontológicos, Paraná, Brazil. Available: https://www.angelusdental.com/img/arquivos/mta_fillapex_bula.pdf.
37. Simon V. Structural and corrosion properties of sodium-calcium-phosphate glasses. Int J Mod Phys B. 2003;17:5849–54.
38. Varshneya AK. Fundamentals of inorganic glasses. London, England: Academic Press Inc; 1994.
39. Goberis S, Antonovich V. Influence of sodium silicate amount on the setting time and EXO temperature of a complex binder consisting of high-aluminate cement, liquid glass and metallurgical slag. Cem Concr Res. 2004;34:1939–41. https://doi.org/10.1016/j.cemconres.2004.01.004.
40. Grover LM, Gbureck U, Wright AJ, Tremayne M, Barralet JE. Biologically mediated resorption of brushite cement in vitro. Biomaterials. 2006;27:2178–85. https://doi.org/10.1016/j.biomaterials.2005.11.012.
41. Chailertvanitkul P, Abbott P, Riley T, Sooksuntisakoonchai N. Bacterial and dye penetration through interim restorations used during endodontic treatment of molar teeth. J Endod. 2009;35:1017–22.
42. Torabinejad M, Watson TF, Ford TRP. Sealing ability of mineral trioxide aggregate when used as a root end filling material. J Endod. 1993;19:591–5.
43. Wu M, kontakiotis E, Wesselink P. Long-term seal provided by some root-end filling materials. J Endod. 1998;24:557–60.
44. Fischer E, Arens D, Miller C. Bacterial leakage of mineral trioxide aggregate as compared with zinc-free amalgam, intermediate restorative material, and Super-EBA as a root-end filling material. J Endod. 1998;24:176–9.